Supporting information for:

Impact of Linking Groups in Chelating Bis-carbene Iridium Catalysts for Transfer Hydrogenation of Inorganic Carbonates with Glycerol

Marvin L. Richter, Eduardo Peris and Sergio Gonell*

Institute of Advanced Materials (INAM), Centro de Innovación en Química Avanzada (ORFEO-CINQA)

Universitat Jaume I

Av. Vicente Sos Baynat s/n. Castellón, E-12071 (Spain)

1. Experimental Details

1.1. General considerations All operations were carried out by using standard Schlenk techniques under nitrogen atmosphere unless otherwise stated.[1] MeCN and CH_2Cl_2 were dried and degassed with a solvent purification system (SPS M BRAUN). The other solvents were used as received from commercial suppliers and kept under air.

D_2O and DMSO-d_6 were purchased from Cambridge Isotope Laboratories Inc. and used as received. **[Ph-bis-mim-H$_2$][PF$_6$]$_2$**,[2] **[C$_2$H$_4$-bis-mim-H$_2$][Br]$_2$**,[3] **[C$_2$H$_4$-bis-mim-H$_2$][PF$_6$]$_2$**,[3] [IrCl(COD)]$_2$[4] and **^{Me}Im-Ir^{2+}**[5] were synthesized according to reported procedures. $Ba(OH)_2 \cdot 8H_2O$ (≥99.9% purity), K_2CO_3 (99% purity), and glycerol (≥99.5% purity) were acquired from Merck and used as received.

All other materials were commercially available and used as received, unless otherwise noted. NMR spectra were recorded on a Bruker 300 MHz or 400 MHz spectrometer at 30 °C. Chemical shifts are reported with respect to residual organic solvents.[6]

Infrared spectra (FTIR) were recorded on a Bruker Equinox 55 spectrometer with a spectral window of 4000-400 cm^{-1}. Electrospray mass spectra (ESI-MS) were recorded on a Micromass Quatro LC instrument; nitrogen was employed as drying and nebulizing gas. Exact mass analyses were recorded by using a Q-TOF Premier mass spectrometer with an electrospray source (Waters, Manchester, UK) operating at a resolution of about 16000 FWHM.

1.2. Synthesis of ^{Me}Ph-Ir$^+$. [IrCl(COD)]$_2$ (50 mg, 74.4 µmol, 1.0 eq.), NaOAc (54 mg, 0.658 mmol, 8.8 eq.) and **[Ph-bis-mim-H$_2$][PF$_6$]$_2$** (80 mg, 0.151 mmol, 2.0 eq.) were dissolved in acetonitrile (20 mL). The solution was heated upon reflux for 2 h changing the colour from yellow to red. After cooling to room temperature, the suspension was filtrated *via* an oven-dried cannula fitted with a paper filter, and then the solvent was removed *in vacuo*. 15 mL of DCM were added to the solid, and the suspension was filtrated over a 0.2 µm Nylon-filter. CO gas was bubbled through the solution for 10 minutes, while a change of colour to yellow was observed. Precipitation with pentane and the subsequent recrystallization through slow diffusion of pentane into a saturated solution of the crude in DCM enabled the isolation of the desired product as yellow crystals (49.0 mg, 77.6 µmol, 52% yield). ^{1}H NMR (400 MHz, DMSO-d_6): δ = 7.90 (d, 2 H, $^3J_{H–H}$ = 2.0 Hz, CH_{Im}), 7.79 (d, 2 H, $^3J_{H–H}$ = 2.0 Hz, CH_{Im}), 7.74 (m, 4 H, CH_{Ph}), 3.89 (s, 6 H, CH_3) ppm. ^{13}C {^{1}H} NMR (101 MHz, DMSO-d_6): δ = 181.6

(Ir–*C*O), 168.9 (Ir–*C*), 131.8 (*C*$_{Ph}$), 130.4 (*C*H$_{Ph}$), 127.4 (*C*H$_{Ph}$), 125.2 (*C*H$_{Im}$), 124.7 (*C*H$_{Im}$), 38.4 (N*C*H$_3$) ppm. HRMS (ESI, m/z): 487.0756 $[M–PF_6]^+$ (calculated: 487.0746).

1.4. Synthesis of $^{Me}C_2H_4$-Ir$^+$. This compound can be synthesized following two different synthetic approaches, which provide the same complex but with different counter ions. **Method A** (PF_6^- counter-anion, **$^{Me}C_2H_4$-Ir$^+$**): **[C_2H_4-bis-mim-H$_2$][PF_6]$_2$** (72 mg, 0.149 mmol, 2.0 eq.), NaOAc (50 mg, 0.610 mmol, 8.2 eq.) and $[IrCl(COD)]_2$ (50 mg, 74.4 µmol, 1.0 eq.) were dissolved in 20 mL acetonitrile and heated upon reflux for 3 h. The red solution was dried *in vacuo* and extracted *via* an oven-dried cannula fitted with a filter paper (20 mL DCM). CO gas was bubbled through the solution, and an immediate darkening was observed. After 10 min, the solution turned green, and the crude was precipitated by adding 30 mL of pentane. The solution was decanted, and the residue extracted with DCM (3 x 3 mL) and filtrated over a 0.2 µm Nylon-filter. After drying *in vacuo,* the product was isolated as a dark yellow powder (47 mg, 80.6 µmol, 54% yield). ^{1}H NMR (400 MHz, DMSO-*d*$_6$): δ = 7.53 (d, 2 H, $^3J_{H–H}$ = 1.9 Hz, C*H*$_{Im}$), 7.51 (d, 2 H, $^3J_{H–H}$ = 1.9 Hz, C*H*$_{Im}$), 5.16–4.34 (*b*d, 4 H C*H*$_2$), 3.80 (s, 6 H, C*H*$_3$) ppm. ^{13}C {^{1}H} NMR (101 MHz, DMSO-*d*$_6$): δ = 181.5 (Ir–*C*O), 165.3 (Ir–*C*), 124.2 (*C*H$_{Im}$), 123.7 (*C*H$_{Im}$), 47.5 (*C*H$_2$), 38.6 (*C*H$_3$) ppm. HRMS (ESI, m/z): 439.0757 $[M–PF_6]^+$ (calculated: 439.0746). **Method B** (Br^- counter-anion, **[$^{Me}C_2H_4$-Ir][Br]**): **[C_2H_4-bis-mim-H$_2$][Br]$_2$** (115 mg, 0.327 mmol, 2.0 eq.) and Ag_2O (91 mg, 0.393 mmol, 1.2 eq.) were suspended in DCM (20 mL), and the solution was stirred overnight at room temperature in the absence of light. $[IrCl(COD)]_2$ (110 mg, 0.164 mmol, 1.0 eq.) was added and the solution was heated upon reflux for 4 h. Under aerobic conditions, the red solution was filtrated through celite, and CO gas was bubbled through the solution at 0 °C for 10 min, changing the colour of the solution to yellow. The crude was precipitated with hexane and the solid collected by filtration. Crystallization, by slow diffusion of hexane into a solution of the crude in acetone at 5 °C, enabled the isolation of **[$^{Me}C_2H_4$-Ir][Br]** as a crystalline yellow powder (43 mg, 82.9 µmol, 25% yield). ^{1}H NMR (400 MHz, DMSO-*d*$_6$): δ = 7.53 (s, 2 H, C*H*$_{Im}$), 7.52 (s, 2 H, C*H*$_{Im}$), 4.87 (*b*m, 2 H, NC*H*$_2$), 4.61 (*b*m, 2 H, NC*H*$_2$), 3.80 (s, 6 H, C*H*$_3$) ppm. ^{13}C {^{1}H} NMR (101 MHz, DMSO-*d*$_6$): δ = 181.5 (Ir–*C*O), 165.2 (Ir–*C*), 124.2 (*C*H$_{Im}$), 123.8 (*C*H$_{Im}$), 47.5 (*C*H$_2$), 38.6 (*C*H$_3$) ppm. HRMS (ESI, m/z): 439.0751 $[M–Br]^+$ (calculated: 439.0746).

2. NMR spectra

2.1 ^{1}H, ^{13}C and HSQC NMR spectra of ^{Me}Ph-Ir^{+}

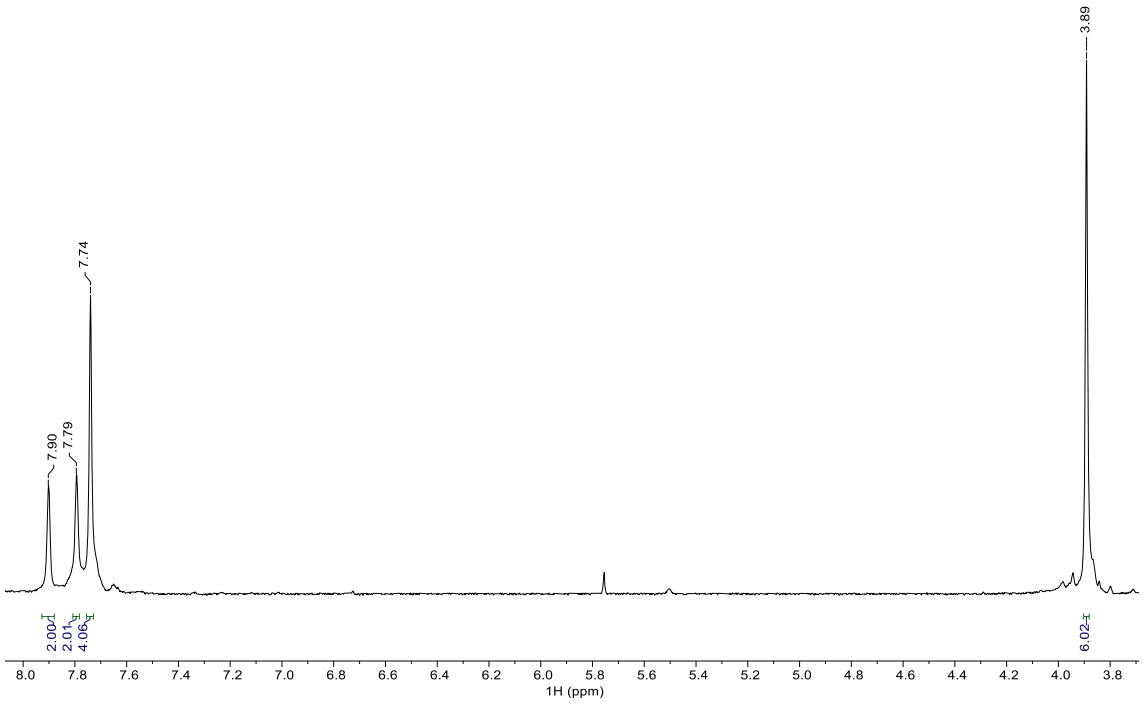

Figure S1. ^{1}H NMR spectrum of ^{Me}**Ph-Ir**$^{+}$ in DMSO-*d*$_6$, 400 MHz.

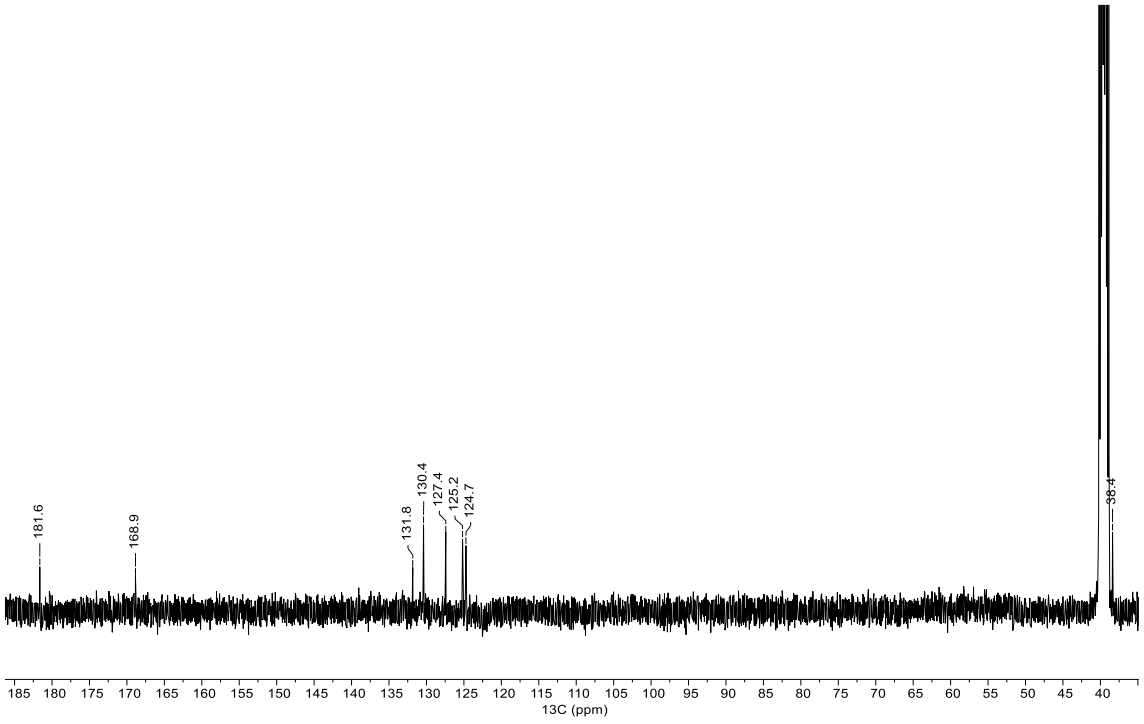

Figure S2. ^{13}C {^{1}H} NMR spectrum of ^{Me}**Ph-Ir**$^{+}$ in DMSO-*d*$_6$, 101 MHz.

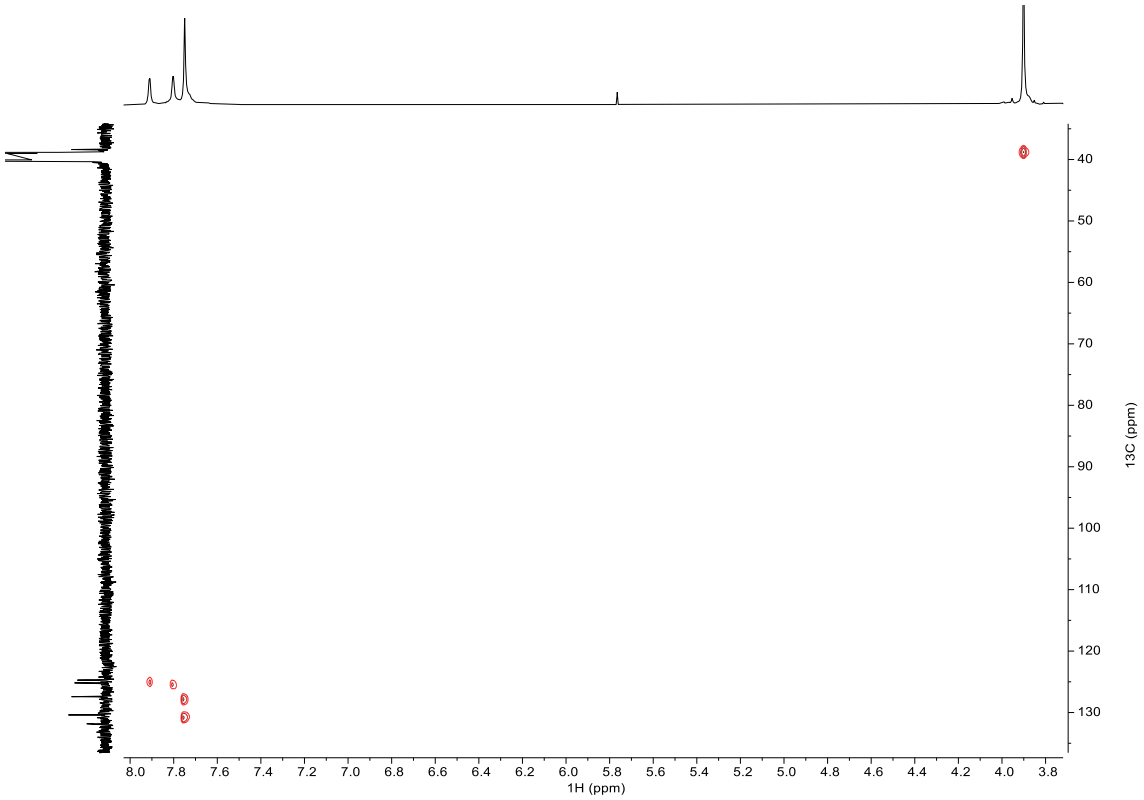

Figure S3. ^{1}H-^{13}C HSQC NMR spectrum of **^{Me}Ph-Ir^{+}** in DMSO-*d*$_6$, 400 MHz.

2.2 ^{1}H, ^{13}C and HSQC NMR spectra of [^{Me}C$_2$H$_4$-Ir][Br]

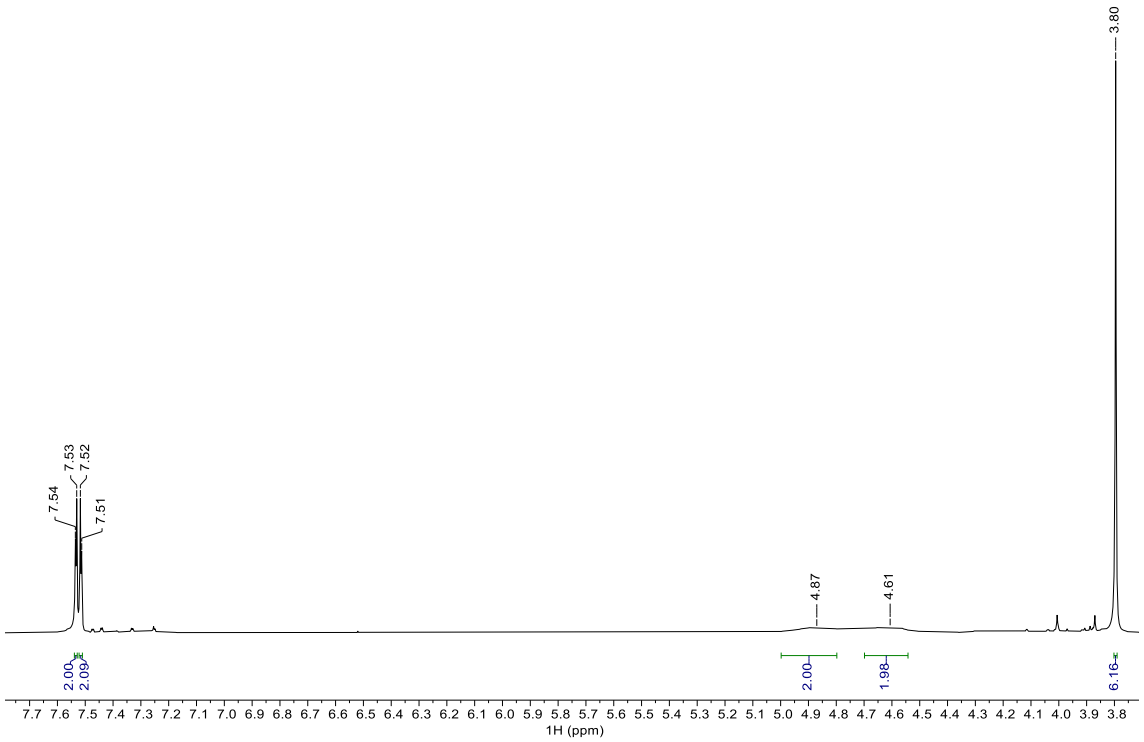

Figure S4. ^{1}H NMR spectrum of **[^{Me}C$_2$H$_4$-Ir][Br]** in DMSO-*d*$_6$, 400 MHz.

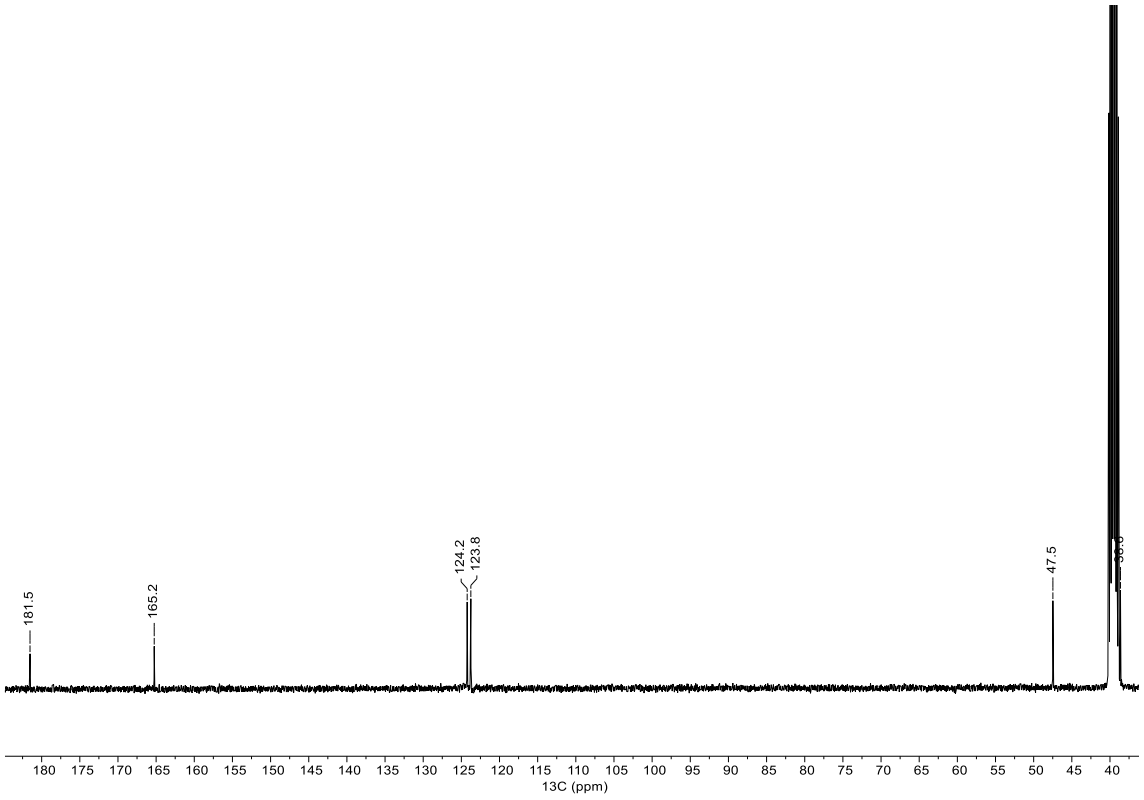

Figure S5. ^{13}C {^{1}H} NMR spectrum of **[$^{Me}C_2H_4$-Ir][Br]** in DMSO-*d*$_6$, 101 MHz.

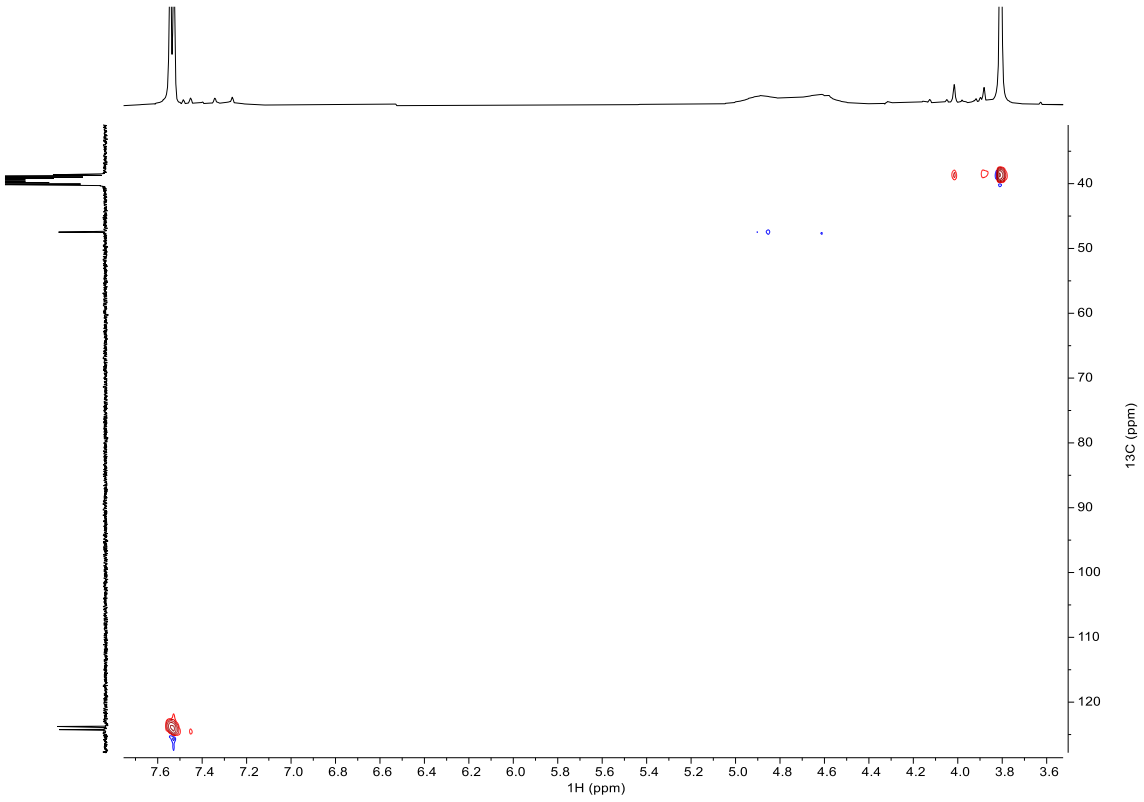

Figure S6. ^{1}H-^{13}C HSQC NMR spectrum of **[$^{Me}C_2H_4$-Ir][Br]** in DMSO-*d*$_6$, 400 MHz.

2.3 ^{1}H, ^{13}C, and HSQC NMR spectra of $^{Me}C_2H_4$-Ir^+

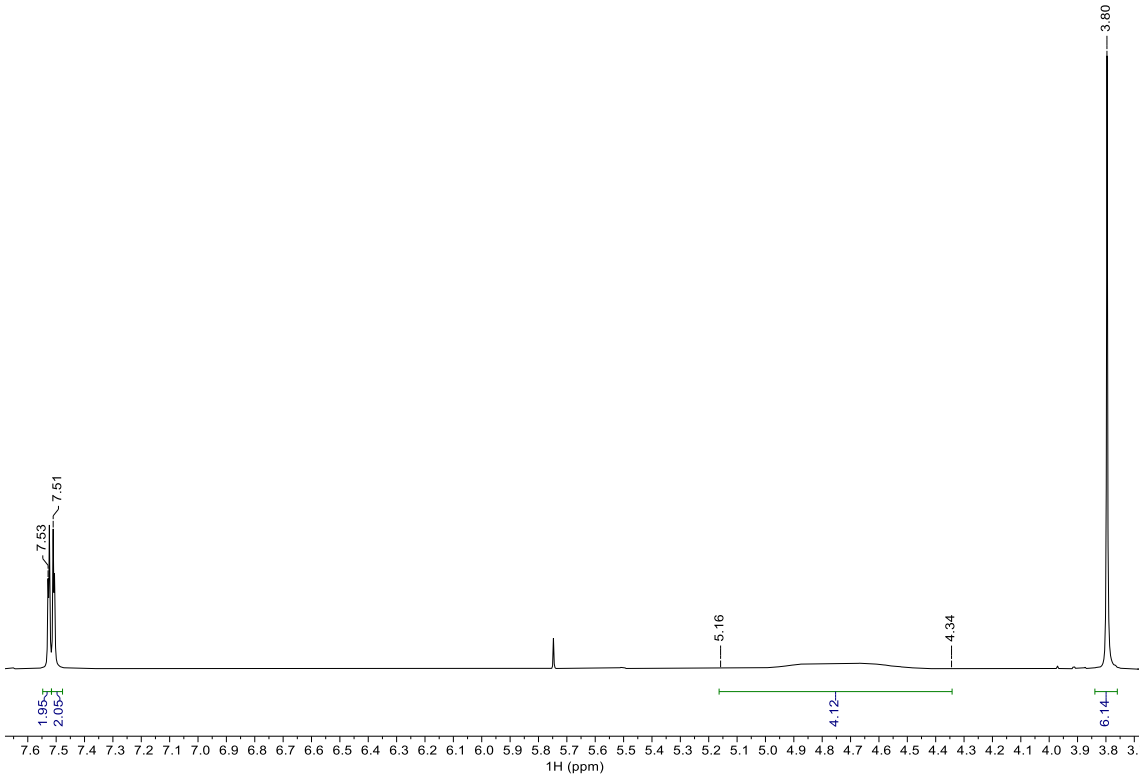

Figure S7. ^{1}H NMR spectrum of $^{Me}C_2H_4$-Ir^+ in DMSO-*d*$_6$, 400 MHz.

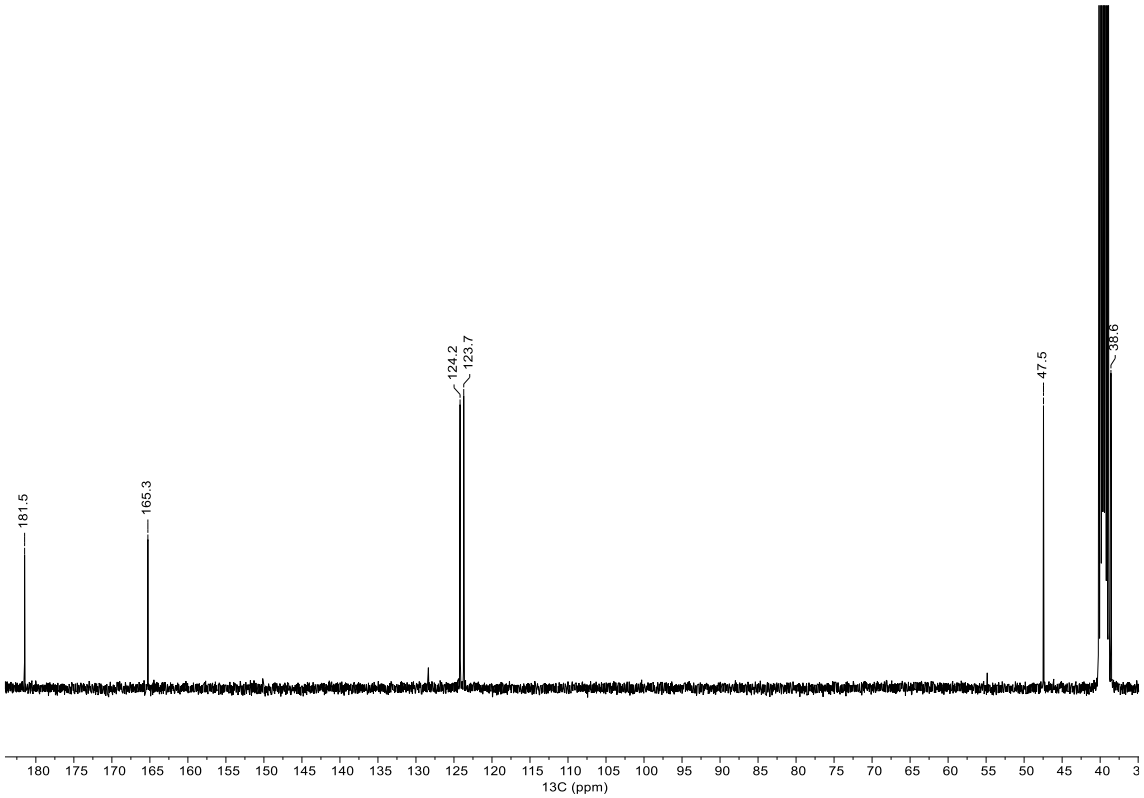

Figure S8. ^{13}C {^{1}H} NMR spectrum of $^{Me}C_2H_4$-Ir^+ in DMSO-*d*$_6$, 101 MHz.

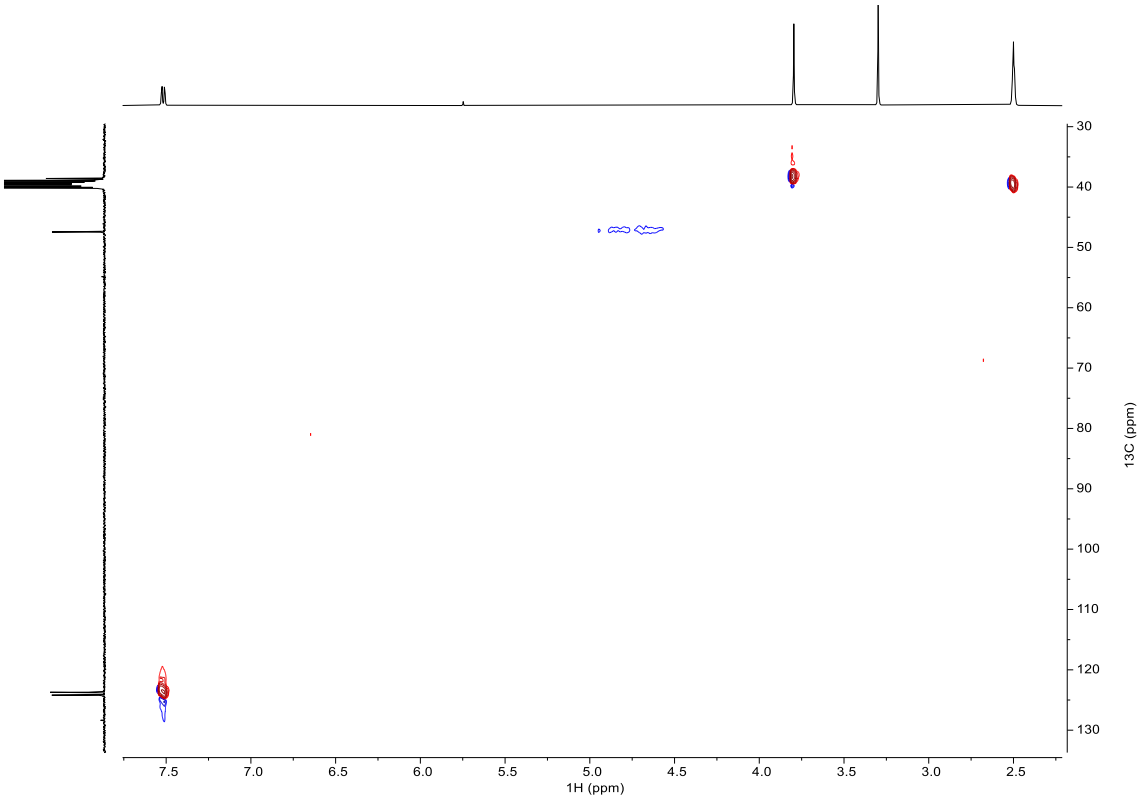

Figure S9. ^{1}H-^{13}C HSQC NMR spectrum of $^{Me}C_2H_4$-Ir^{+} in DMSO-d_6, 400 MHz.

3. IR Spectra

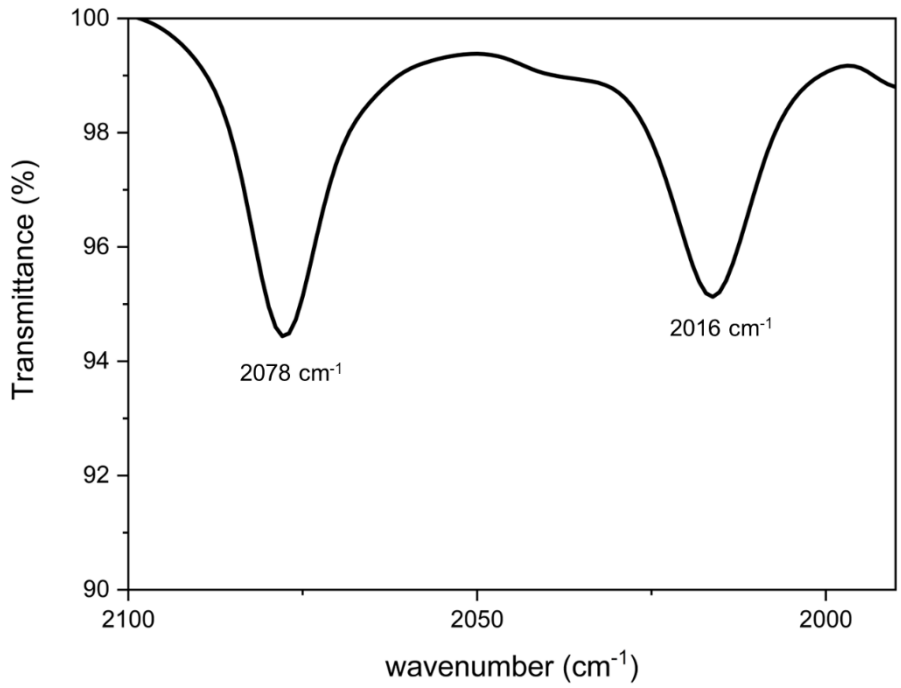

Figure S10. IR spectrum of ^{Me}**Im-Ir**$^{2+}$ in acetonitrile.

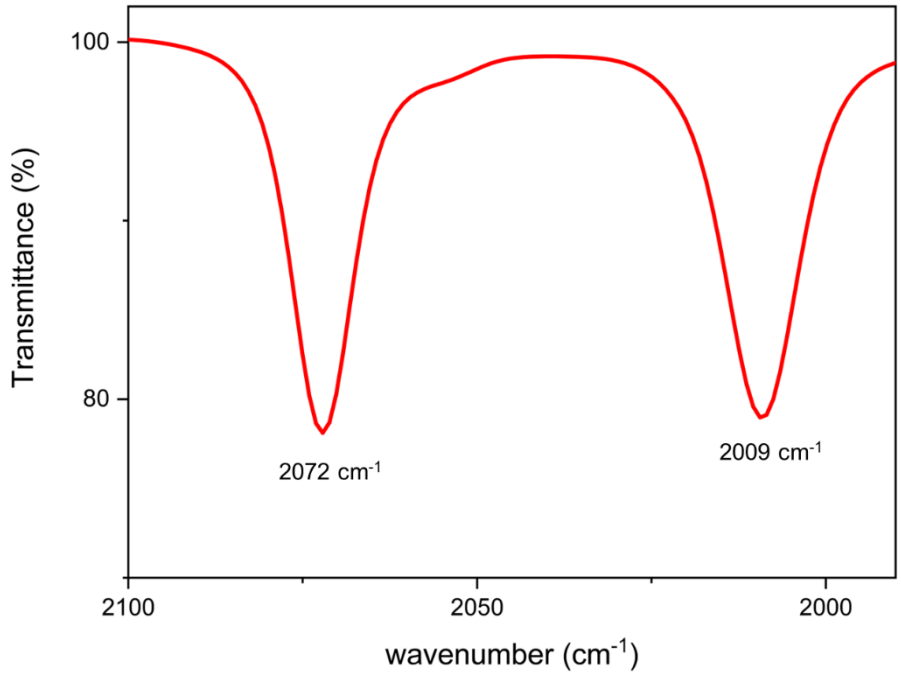

Figure S11. IR spectrum of ^{Me}**Ph-Ir**$^{+}$ in acetonitrile.

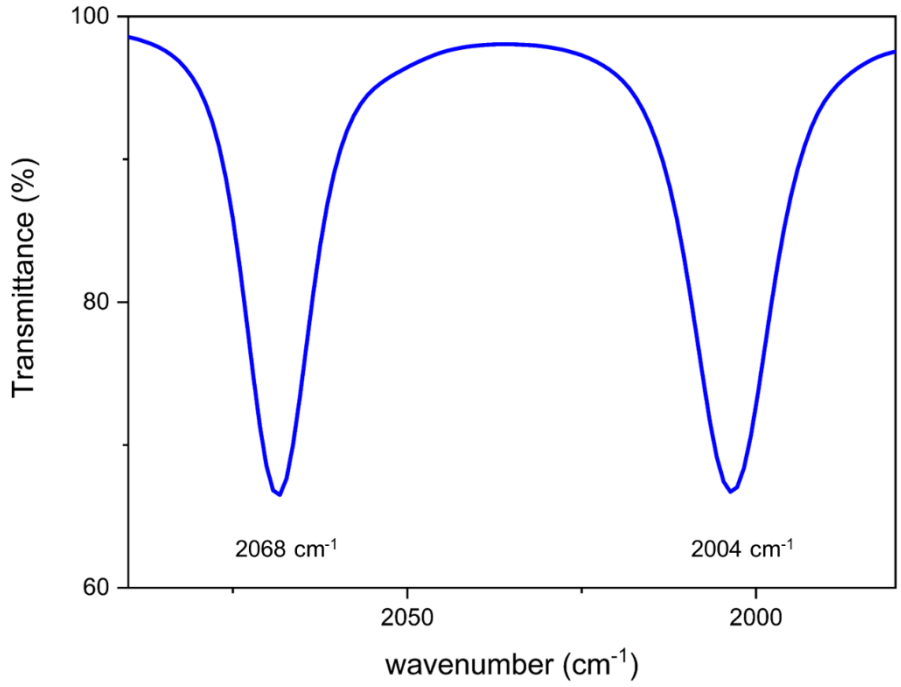

Figure S12. IR spectrum of **[$^{Me}C_2H_4$-Ir][Br]** in acetonitrile.

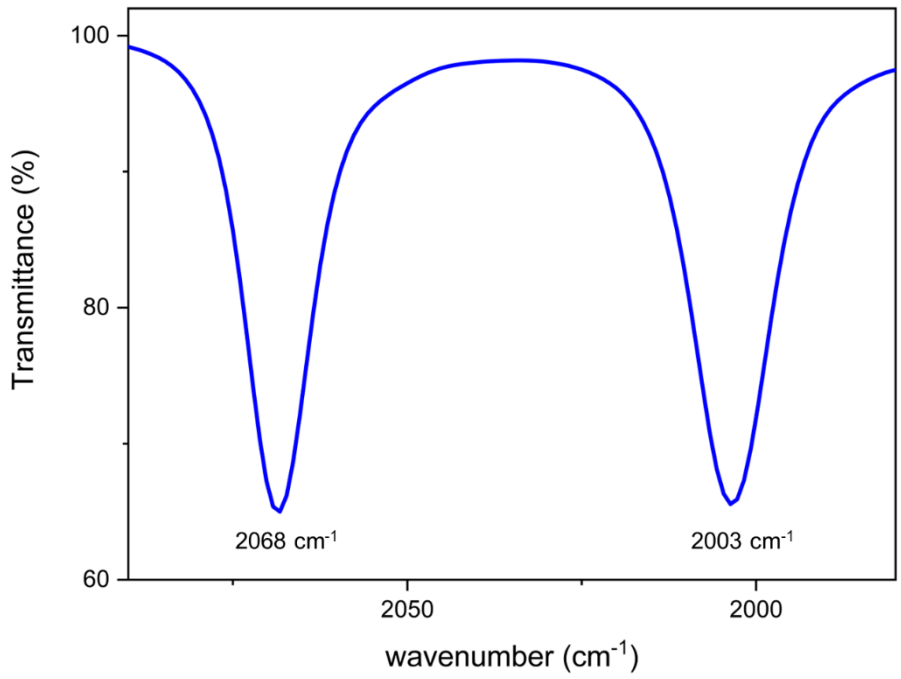

Figure S13. IR spectrum of **$^{Me}C_2H_4$-Ir$^+$** in acetonitrile.

4. Electrochemical methods

4.1. Electrochemical measurements

Electrochemical studies were performed using an Autolab Potentiostat, Model PGSTAT101 controlled with NOVA 2.1.6 software. All the solutions were deoxygenated by sparging with Ar for at least 15 min. Tetrabutylammonium hexafluorophosphate ($TBAPF_6$, Sigma Aldrich, electrochemical grade) was used as electrolyte (100 mM) in all experiments. MeCN was dried and degassed with a solvent purification system (SPS M BRAUN, < 20 ppm residual H_2O, measured by Karl Fischer titration).

Cyclic voltammetry was performed in an undivided three-electrode cell with a 3 mm diameter disk glassy carbon working electrode, a platinum counter electrode, and a silver wire pseudo-reference electrode. The glassy carbon working electrode (CH Instruments) was polished between scans with 0.05-μm alumina powder (CH Instruments, contained no agglomeration agents) before rinsing with miliQ water and acetone. All scans were referenced to the ferrocenium/ferrocene (Fc^+/Fc) couple at 0 V. Ferrocene was present in each scan. Ohmic drop was minimized by minimizing the distance between the working and reference electrodes. The residual ohmic drop was estimated by positive feedback and compensated at 90%.

The normalized scan rate dependent CVs were built taking into account the Randles−Sevcik equation, dividing the current of the sweep by the square root of the scan rate. The Randles−Sevcik equation describes how the peak current i_p (A) increases linearly with the square root of the scan rate υ ($V \cdot s^{-1}$), for an electrochemically reversible electron transfer process involving freely diffusing species. n is the number of electrons transferred in the redox event, A (cm^2) is the electrode surface area, D_0 ($cm^2 \cdot s^{-1}$) is the diffusion coefficient of the analyte, and C^0 ($mol \cdot cm^{-3}$) is the bulk concentration of the analyte.

$$i_p = 0.446nFAC^0 \left(\frac{nF\upsilon D_0}{RT}\right)^{1/2} \text{ (Eq. S1)}$$

4.2 Electrochemical kinetic analysis

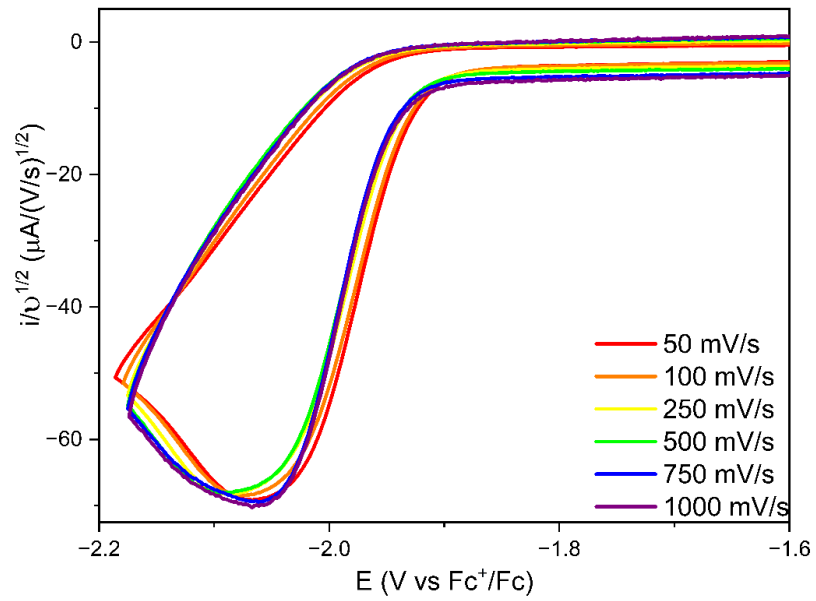

Figure S14. Normalized CV of $^{Me}C_2H_4$-Ir^+ under Ar in MeCN from 50 mV/s to 1000 mV/s. Conditions: Ar atmosphere, MeCN, [Ir] = 1 mM, [$TBAPF_6$] = 100 mM, 3 mm glassy carbon disc working electrode, Pt wire counter electrode, Ag wire pseudo-reference electrode.

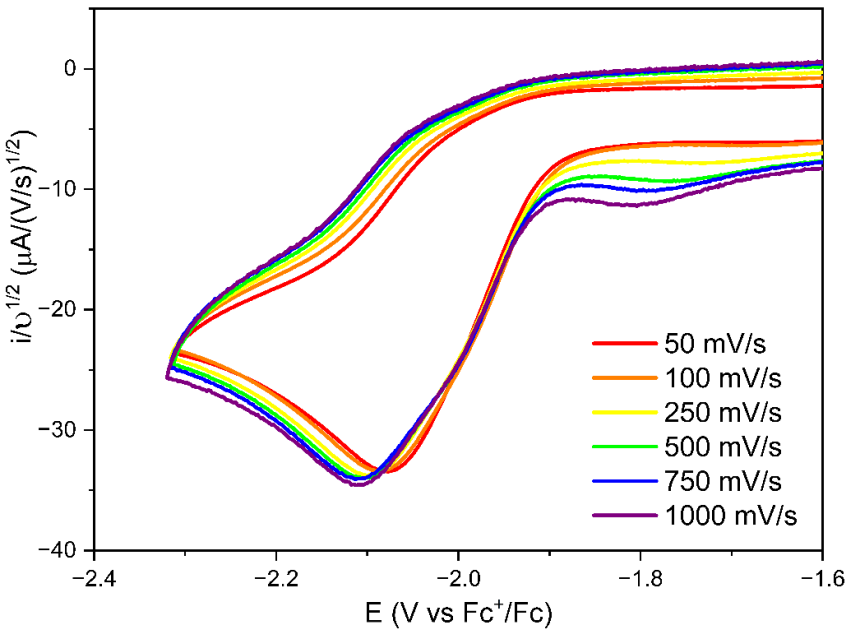

Figure S15. Normalized CV of ^{Me}**Ph-Ir**$^+$ under Ar in MeCN from 50 mV/s to 1000 mV/s. Conditions: Ar atmosphere, MeCN, [Ir] = 1 mM, [$TBAPF_6$] = 100 mM, 3 mm glassy carbon disc working electrode, Pt wire counter electrode, Ag wire pseudo-reference electrode.

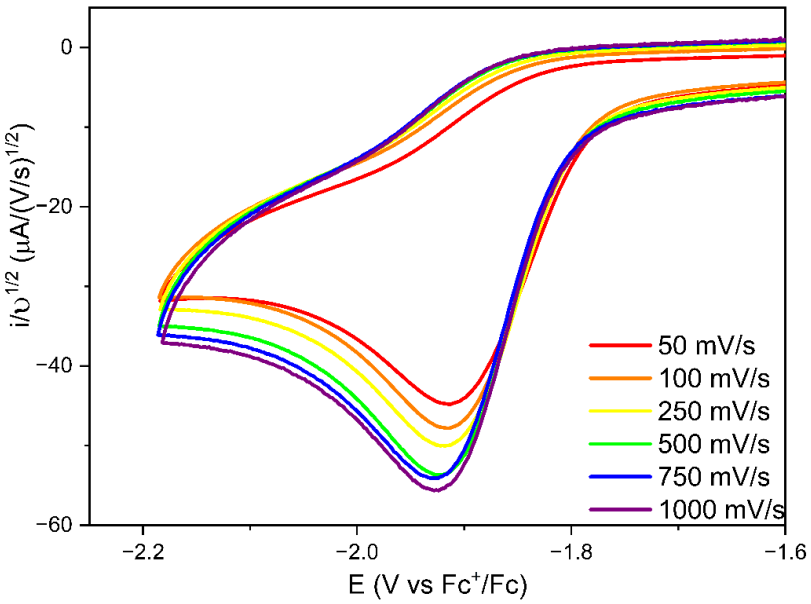

Figure S16. Normalized CV of ^{Me}**Im-Ir**$^{2+}$ under Ar in MeCN from 50 mV/s to 1000 mV/s. Conditions: Ar atmosphere, MeCN, [Ir] = 1 mM, [$TBAPF_6$] = 100 mM, 3 mm glassy carbon disc working electrode, Pt wire counter electrode, Ag wire pseudo-reference electrode.

5. Catalytical experiments

5.1 Catalytical measurements

All measurements were performed under an atmosphere of N_2. MiliQ water was utilized to prepare the stock solution of the complexes for the catalytic experiments. Glycerol was degassed by sonicating it under vacuum for 1 h then flushing it with N_2 and repeating this procedure two more times. Then it was stored under nitrogen in a Schlenk tube. Each experiment was performed at least twice to get a mean and a standard deviation.

4 mmol of K_2CO_3 (553 mg) or $Ba(OH)_2 \cdot 8H_2O$ (1.262 g) were placed either in a Schlenk tube or in a high pressure Schlenk tube fitted with a Teflon cap. The Schlenk tubes were additionally fitted with a reflux condenser and a gas bubbler during the experiment, while the Schlenk tubes fitted with a Teflon cap were sealed. 50 µL stock solution of the catalyst in water (1.5–2.8 mM) were added to the glycerol solution, enabling a catalyst loading between 35 and 280 nmol. When the catalyst was insoluble in water, it was added first to the flask in a stock solution in DCM, dried *in vacuo* and then 50 µL of miliQ water were added. Finally, 1 mL of Glycerol was added. The mixtures were heated to 180 °C for the appropriate amount of time (1–6 or 24 h). Afterwards, the mixture was cooled to room temperature, 9 mL of a stock solution of isonicotinic acid in water (5.3–7.7 mM) was added and, if needed, the mixture was shortly heated with a heat gun to ensure homogeneity. 450 µL of this mixture and 150 µL of D_2O were placed in an NMR tube and measured at a 400 MHz Bruker device with a delay time of 20 s and 32 scans. An example of the typically obtained ^1H spectrum is shown in Figure S17.

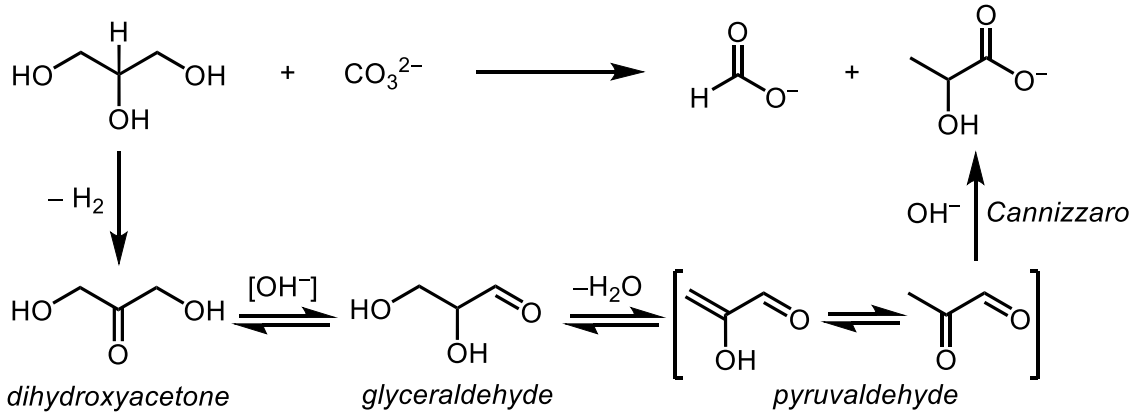

Scheme S1. Overall reactions involved in the transfer hydrogenation of inorganic carbonates with glycerol.

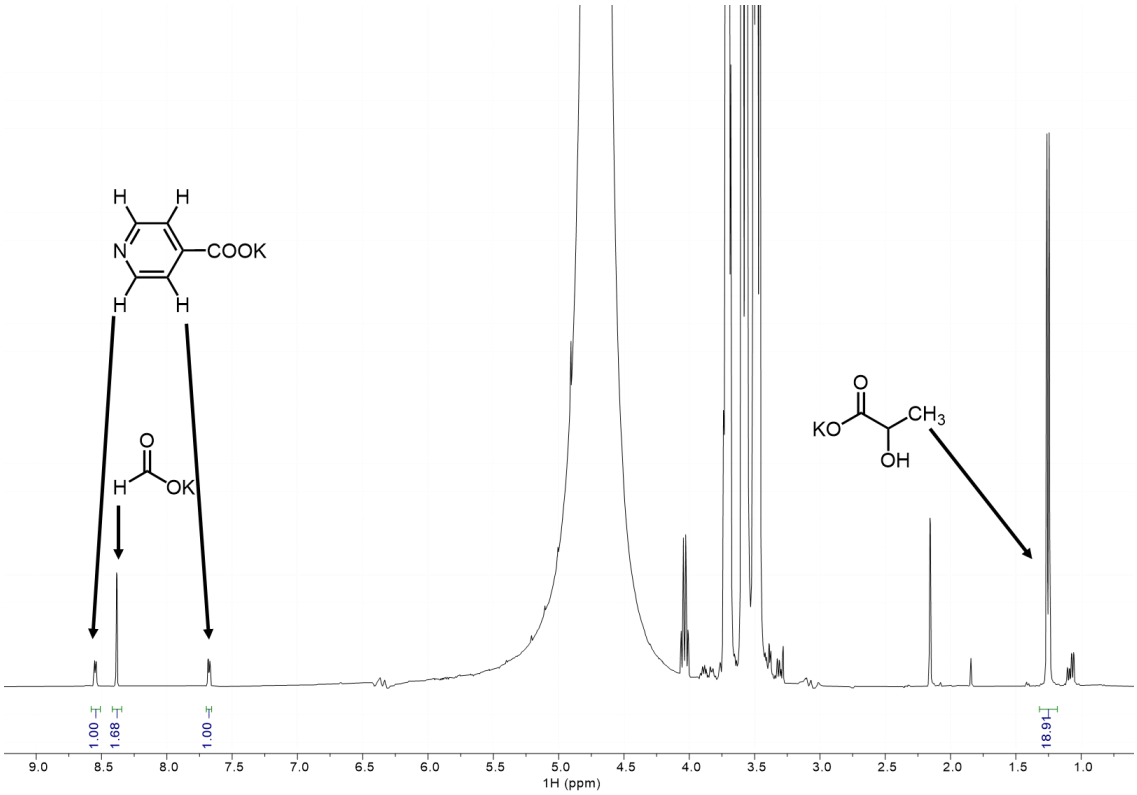

Figure S17. Exemplary ^{1}H NMR spectrum of a catalytic reaction, showing the peaks utilized to calculate the TON (isonicotinate standard, deprotonated due to the basic nature of the mixture, formate and the CH_3-group of lactate). Due to the overlap with the wide peak of water, the CH-peak of lactate was not integrated. The spectrum was not referenced to the shift of the solvent.

5.2 Catalytic Results

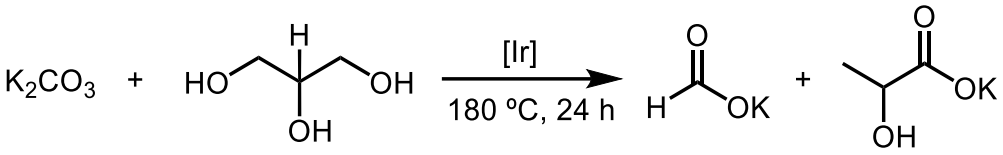

Table S1. Results of the transfer hydrogenation of K_2CO_3 with glycerol.[a]

Entry	Catalyst	TON formate [10^3]	TON lactate [10^4]
1[b]	^{Me}**Im-Ir^{2+}**	7.04 ± 2.04	1.56 ± 0.36
2[b]	^{Me}**Ph-Ir^{+}**	5.05 ± 0.87	1.98 ± 0.22
3[b]	^{Me}**C$_2$H$_4$-Ir^{+}**	3.80 ± 1.05	1.61 ± 0.07
4[b]	**[^{Me}C$_2$H$_4$-Ir][Br]**	4.32 ± 1.48	1.90 ± 0.27
5[c]	^{Me}**Im-Ir^{2+}**	7.23 ± 2.31	1.63 ± 0.52
6[c]	^{Me}**Ph-Ir^{+}**	2.62 ± 0.90	1.83 ± 0.46
7[c]	^{Me}**C$_2$H$_4$-Ir^{+}**	1.91 ± 0.21	1.47 ± 0.03
8[c]	**[^{Me}C$_2$H$_4$-Ir][Br]**	1.98 ± 1.59	2.13 ± 0.31

[a]Reaction conditions: Glycerol (1 mL), K_2CO_3 (4 mmol), 0.14 µmol of Ir catalyst in 50 µL of H_2O, 180 °C, 24 h. [b]Performed in a high pressure Schlenk tube fitted with a Teflon cap. [c]Performed in a Schlenk tube fitted with a reflux condenser and a bubbler.

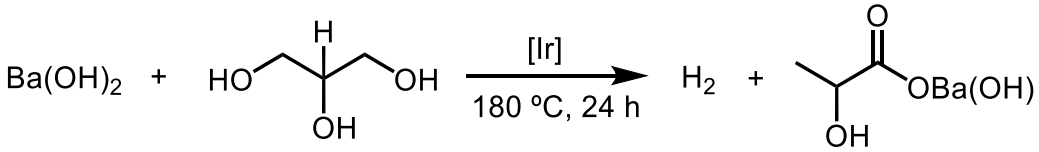

Table S2. Results of glycerol dehydrogenation of $Ba(OH)_2$.[a]

Entry	Catalyst	TON lactate [10^4]
1[b]	^{Me}**Im-Ir^{2+}**	5.71 ± 0.82
2[b]	^{Me}**Ph-Ir^{+}**	5.64 ± 0.36
3[b]	^{Me}**C$_2$H$_4$-Ir^{+}**	5.65 ± 0.87
4[b]	**[^{Me}C$_2$H$_4$-Ir][Br]**	5.74 ± 0.79
5[c]	^{Me}**Im-Ir^{2+}**	5.34 ± 0.26
6[c]	^{Me}**Ph-Ir^{+}**	3.82 ± 1.30
7[c]	^{Me}**C$_2$H$_4$-Ir^{+}**	3.36 ± 1.81
8[c]	**[^{Me}C$_2$H$_4$-Ir][Br]**	4.73 ± 0.89

[a]Reaction conditions: Glycerol (1 mL), $Ba(OH)_2 \cdot 8H_2O$ (4 mmol), 0.14 µmol of Ir catalyst in 50 µL of H_2O, 180 °C, 24 h. [b]Performed in a high pressure Schlenk tube fitted with a Teflon cap. [c]Performed in a Schlenk tube fitted with a reflux condenser and a bubbler.

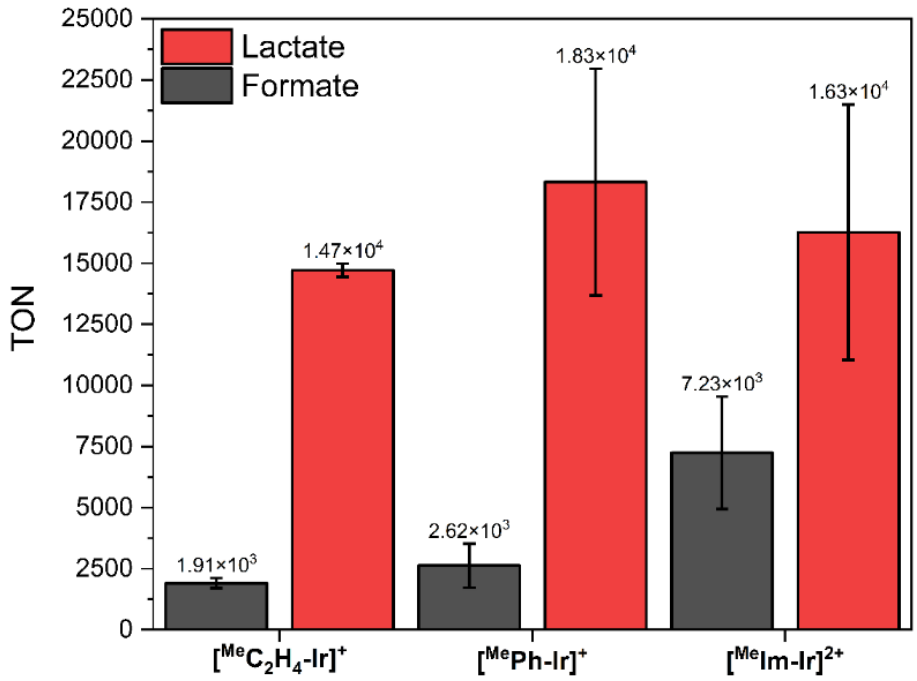

Figure S18. Results of the transfer hydrogenation of K_2CO_3 with glycerol in an open vessel. Reaction conditions: Glycerol (1 mL), K_2CO_3 (4 mmol), 0.14 µmol of Ir catalyst in 50 µL of H_2O, 180 °C, 24 h. Reactions performed in a Schlenk tube fitted with condenser and a bubbler. TONs obtained from the average of at least two independent runs. Uncertainty represents the standard deviation.

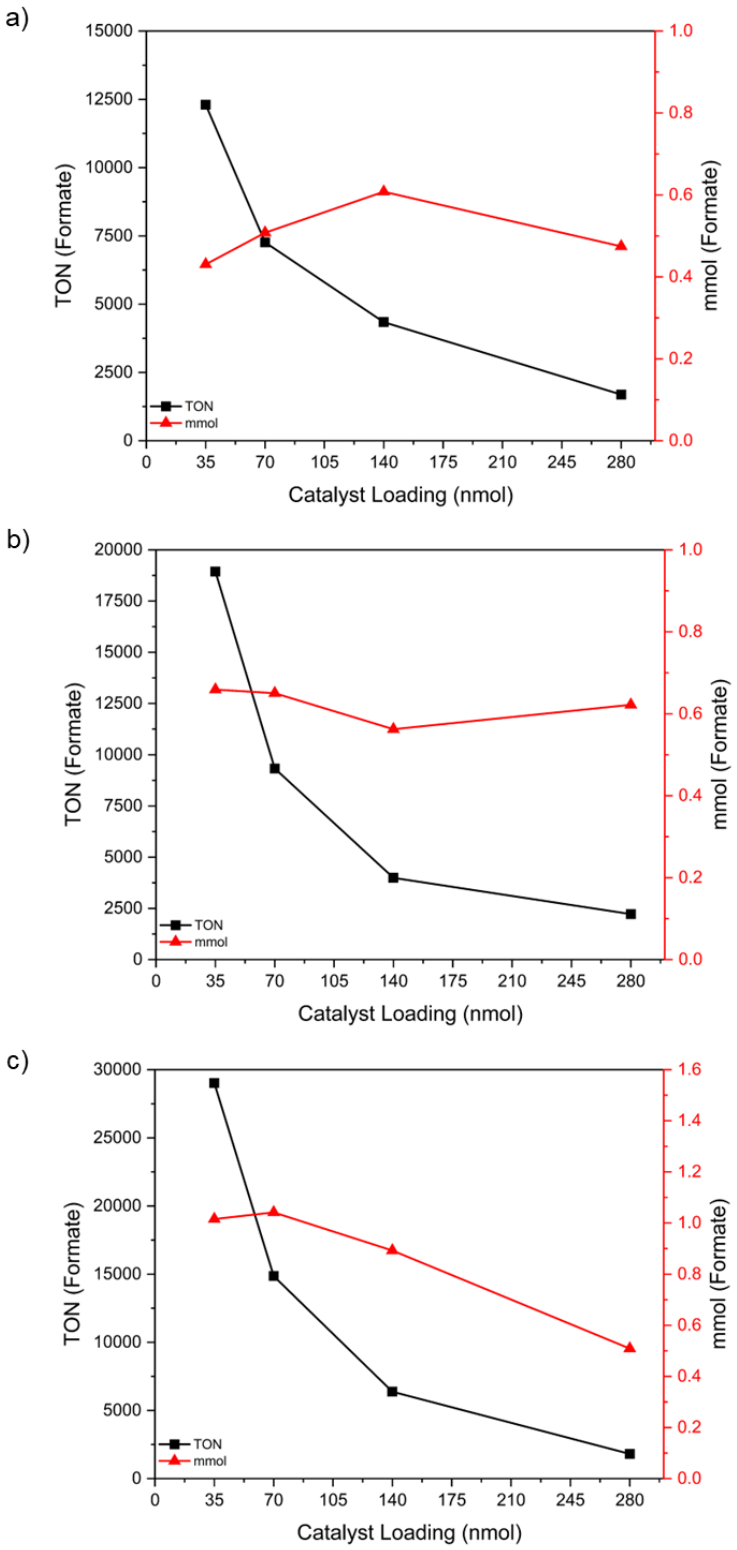

Figure S19. Results of the transfer hydrogenation of K_2CO_3 with glycerol for the generation of formate in a closed vessel, utilizing different catalyst loadings of $^{Me}C_2H_4$-**Ir**$^{+}$ (a), ^{Me}**Ph-Ir**$^{2+}$ (b) or ^{Me}**Im-Ir**$^{2+}$ (c). Reaction conditions: Glycerol (1 mL), K_2CO_3 (4 mmol), 0.14 µmol of Ir catalyst in 50 µL of H_2O, 180 °C, 24 h. Reactions performed in a high pressure Schlenk tube fitted with a Teflon cap

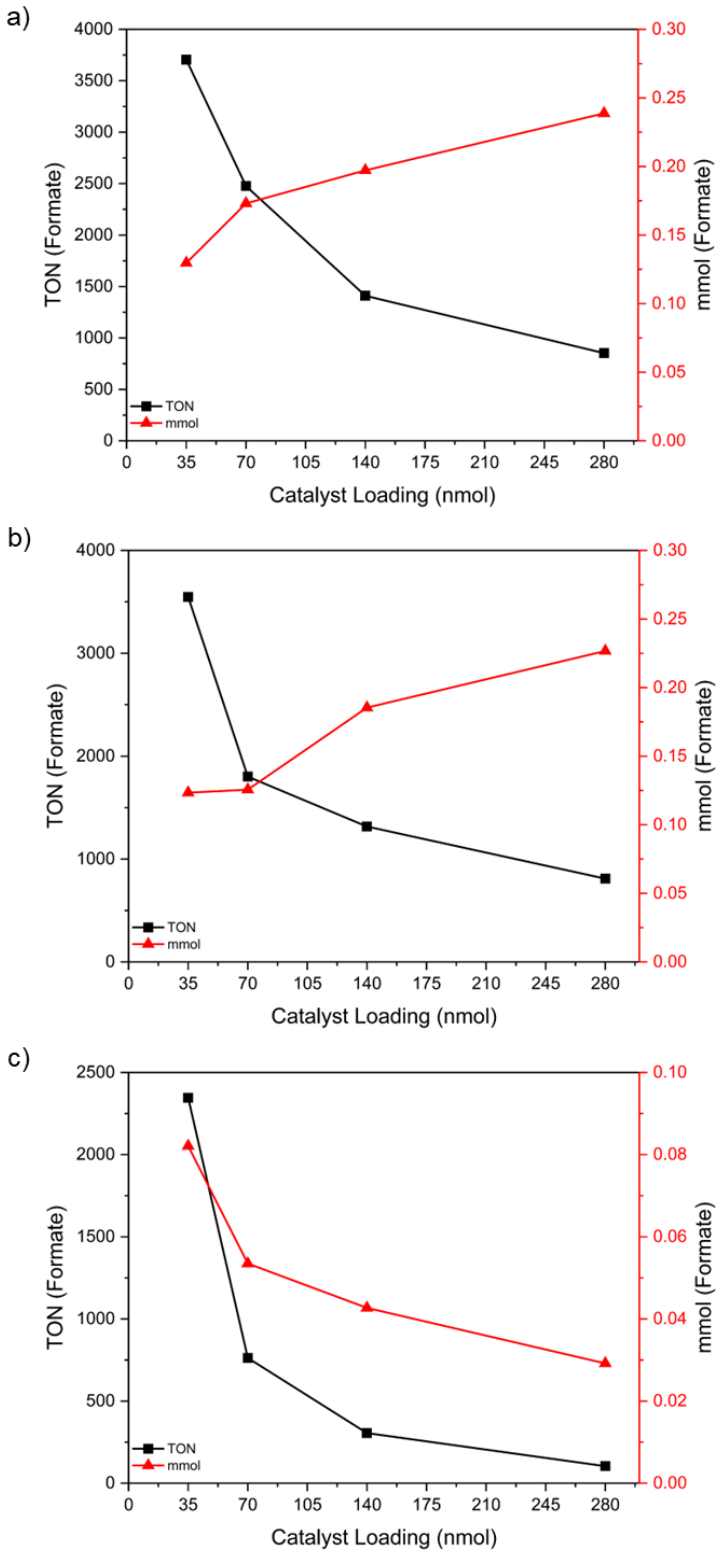

Figure S20. Results of the transfer hydrogenation of K_2CO_3 with glycerol for the generation of formate in a closed vessel, utilizing different catalyst loadings of $^{Me}C_2H_4$-**Ir**$^{+}$ (a), ^{Me}**Ph-Ir**$^{2+}$ (b) or ^{Me}**Im-Ir**$^{2+}$ (c). Reaction conditions: Glycerol (1 mL), K_2CO_3 (4 mmol), 0.14 µmol of Ir catalyst in 50 µL of H_2O, 180 °C, 1 h. Reactions performed in a high pressure Schlenk tube fitted with a Teflon cap.

6. Crystallographic methods

Single-crystal X-ray diffraction data were collected on an Agilent SuperNova diffractometer equipped with an Atlas CCD detector using Cu-K_α radiation (λ = 1.54184 Å). Single crystals were mounted on a MicroMount® polymer tip (MiteGen) in a random orientation. The structures were solved by direct methods using SHELXS and refined with SHELXL[7] with least squares minimization using the Olex2 software package.[8] Data were corrected for absorption effects using the Multi-Scan and the Gaussian method. Non-hydrogen atoms were refined anisotropically. The hydrogen atoms were placed in geometrically calculated positions with Uiso = 1.2Uequiv of the parent atom (Uiso = 1.5Uequiv for methyl). Key details of the crystals and structure refinement data are summarized in Supplementary Tables S3 to S11. Further crystallographic details may be found in the CIF files, which were deposited at the Cambridge Crystallographic Data Centre, Cambridge, UK. The reference numbers for compounds **^{Me}Im-Ir^{2+}**, **^{Me}Ph-Ir^{+}** and **[^{Me}C$_2$H$_4$-Ir][Br]** were assigned as 2465664, 2465665 and 2465666, respectively.

Suitable crystals of **^{Me}Im-Ir^{2+}**, **^{Me}Ph-Ir^{+}** and **[^{Me}C$_2$H$_4$-Ir][Br]** for X-ray diffraction experiments were obtained by slow diffusion of pentane into a saturated solution of the iridium complexes in acetone. For **^{Me}Im-Ir^{2+}**, the diffusion of pentane was in the gas phase and the crystallization took place at room temperature. For **[^{Me}C$_2$H$_4$-Ir][Br]**, the same approach was followed, but at low temperature. For **^{Me}Ph-Ir^{+}**, the two solvents were layered, and the diffusion took place at low temperature.

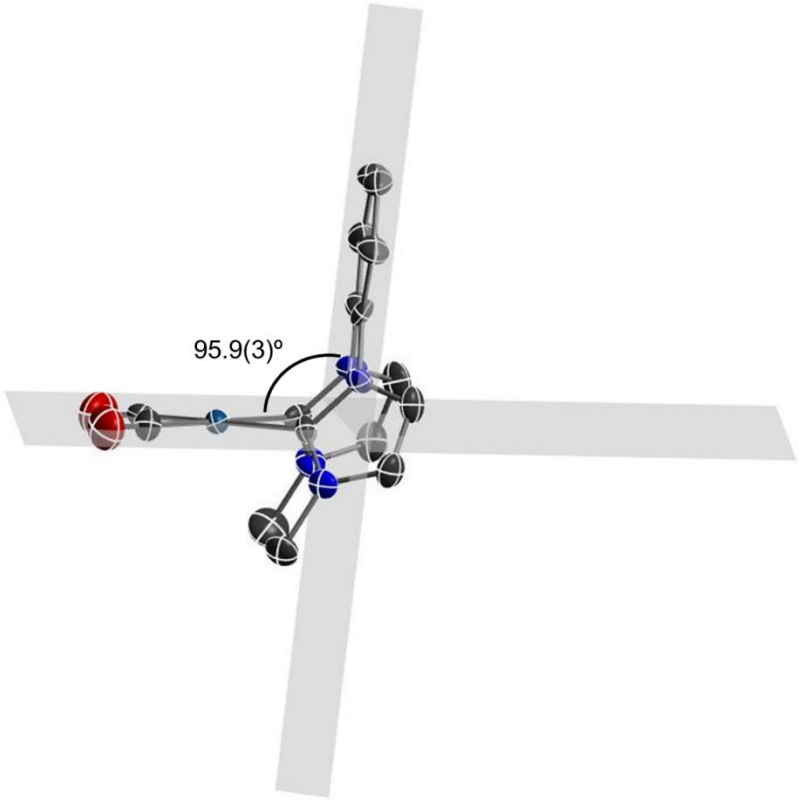

Figure S21. Side-on view of the molecular structure of ^{Me}**Ph-Ir**$^{+}$ displaying the "chair angle".

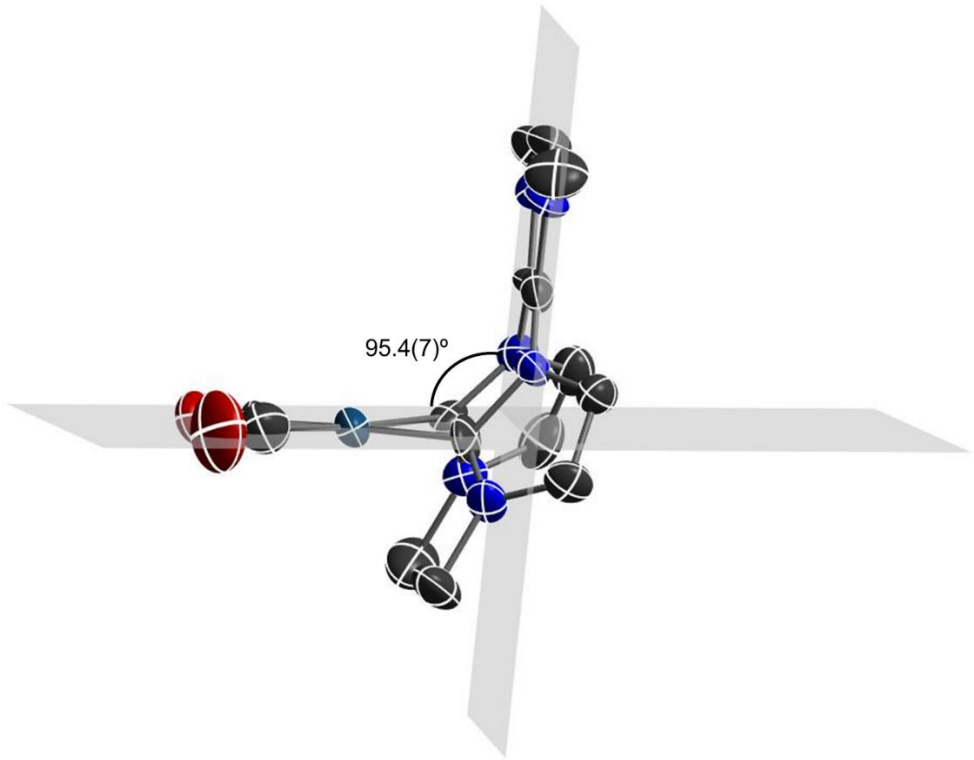

Figure S22. Side-on view of the molecular structure of ^{Me}**Im-Ir**$^{2+}$ displaying the "chair angle".

CheckCIF on Platon on the crystallographic data of **[$^{Me}C_2H_4$-Ir][Br]** shows A type alerts (**PLAT971_ALERT_2_A** and **PLAT972_ALERT_2_A**) concerning *larger than expected residual positive density maximum on the iridium and bromide locations*.

RESPONSE: It is normal to expect the largest residual electron density to be associated with heavy atom sites. While these are larger than expected residual, the data was checked for signs of twinning, using Platon, and no twin law was detected. Next, we have supporting characterizations to indicate that the iridium and bromide atoms have been correctly assigned. Finally, given the proximity to the heavy atoms, it is not likely that these peaks represent solvent, or other small molecules that have been missed.

Moreover, the structure model of **[$^{Me}C_2H_4$-Ir][Br]** shows the following A alert after CheckCIF on Platon:

PLAT434_ALERT_2_A Short Inter HL..HL Contact Br1 ..Br1 (2.93 Å)

PLAT434_ALERT_2_A Short Inter HL..HL Contact Br2 ..Br2 (2.91 Å)

RESPONSE: The bromide ligand contains larger than expected residual density outside the atom locations, therefore, some close contacts between bromide ligands might be expected.

Table S3. Crystal data and structure refinement for ^{Me}**Im-Ir^{2+}**.

Identification code	str2311_auto
Empirical formula	$C_{18}H_{23}B_2F_8IrN_6O_3$
Formula weight	737.24
Temperature/K	240(2)
Crystal system	monoclinic
Space group	$P2_1$
a/Å	10.3330(2)
b/Å	10.8804(2)
c/Å	12.1379(3)
α/°	90
β/°	106.579(2)
γ/°	90
Volume/Å^3	1307.90(5)
Z	2
ρ_{calc}g/cm^3	1.872

μ/mm^{-1}	10.712
F(000)	712.0
Crystal size/mm^3	0.371 × 0.099 × 0.071
Radiation	Cu Kα (λ = 1.54184)
2Θ range for data collection/°	7.6 to 133.196
Index ranges	$-12 \leq h \leq 12$, $-9 \leq k \leq 12$, $-12 \leq l \leq 14$
Reflections collected	9457
Independent reflections	3729 [R_{int} = 0.0194, R_{sigma} = 0.0202]
Data/restraints/parameters	3729/270/347
Goodness-of-fit on F^2	1.040
Final R indexes [I>=2σ (I)]	R_1 = 0.0329, wR_2 = 0.0879
Final R indexes [all data]	R_1 = 0.0343, wR_2 = 0.0898
Largest diff. peak/hole / e $Å^{-3}$	1.44/-1.00
Flack parameter	0.473(18)

Table S4. Bond lengths for ^{Me}**Im-Ir**$^{2+}$.

Atom	Atom	Length/Å	Atom	Atom	Length/Å
Ir_1	C_3	1.93(2)	C_7	C_6	1.45(3)
Ir_1	C_2	2.06(2)	N_6	C_9	1.40(2)
Ir_1	C_4	1.89(3)	N_6	C_{10}	1.37(3)
Ir_1	C_1	2.12(2)	N_6	C_8	1.49(3)
F_7	B_2	1.334(13)	N_5	C_{11}	1.37(2)
C_3	O_2	1.08(3)	N_5	C_{10}	1.27(3)
C_2	N_2	1.33(3)	N_5	C_{12}	1.45(3)
C_2	N_1	1.40(2)	C_{11}	C_9	1.346(11)
C_4	O_1	1.14(4)	F_8	B_2	1.40(3)
C_1	N_3	1.40(2)	F_5	B_2	1.30(3)
C_1	N_4	1.24(3)	F_6	B_2	1.350(13)
N_3	C_7	1.32(3)	F_2	B_1	1.346(13)
N_3	C_9	1.39(3)	F_3	B_1	1.24(3)
N_2	C_{11}	1.39(3)	F_4	B_1	1.36(3)
N_2	C_{13}	1.45(3)	B_1	F_1	1.467(17)
N_4	C_5	1.46(3)	C_{13}	C_{14}	1.18(3)
N_4	C_6	1.41(3)	C_{16}	C_{17}	1.89(4)
N_1	C_{15}	1.49(3)	C_{18}	C_{17}	1.92(5)
N_1	C_{14}	1.38(3)			

Table S5. Bond angles for ^{Me}**Im-Ir**$^{2+}$.

Atom	Atom	Atom	Angle/°	Atom	Atom	Atom	Angle/°
C_3	Ir_1	C_2	88.8(11)	C_{10}	N_6	C_9	105.1(16)
C_3	Ir_1	C_1	175.2(12)	C_{10}	N_6	C_8	128.5(16)
C_2	Ir_1	C_1	87.1(3)	C_{11}	N_5	C_{12}	127.6(18)
C_4	Ir_1	C_3	92.0(4)	C_{10}	N_5	C_{11}	109.7(17)
C_4	Ir_1	C_2	175.9(12)	C_{10}	N_5	C_{12}	122.7(17)
C_4	Ir_1	C_1	92.2(13)	N_5	C_{11}	N_2	126(2)
O_2	C_3	Ir_1	178(2)	C_9	C_{11}	N_2	126(2)
N_2	C_2	Ir_1	128.4(14)	C_9	C_{11}	N_5	108(2)
N_2	C_2	N_1	101.9(18)	N_3	C_9	N_6	120.6(18)
N_1	C_2	Ir_1	129.2(15)	C_{11}	C_9	N_3	132(2)
O_1	C_4	Ir_1	174(3)	C_{11}	C_9	N_6	107(2)
N_3	C_1	Ir_1	121.8(15)	N_5	C_{10}	N_6	110.4(6)
N_4	C_1	Ir_1	130.7(16)	F_7	B_2	F_8	103.1(18)
N_4	C_1	N_3	107.4(19)	F_7	B_2	F_6	102.8(12)
C_7	N_3	C_1	109.8(16)	F_5	B_2	F_7	118(2)
C_7	N_3	C_9	125.7(16)	F_5	B_2	F_8	114.0(9)
C_9	N_3	C_1	123.8(17)	F_5	B_2	F_6	108.8(19)
C_2	N_2	C_{11}	121.4(16)	F_6	B_2	F_8	110(2)
C_2	N_2	C_{13}	110.7(16)	F_2	B_1	F_4	111(3)
C_{11}	N_2	C_{13}	127.9(17)	F_2	B_1	F_1	105.4(10)
C_1	N_4	C_5	127.4(19)	F_3	B_1	F_2	119.2(19)
C_1	N_4	C_6	113.6(17)	F_3	B_1	F_4	114.4(13)
C_6	N_4	C_5	118.8(18)	F_3	B_1	F_1	118(2)
C_2	N_1	C_{15}	122.0(18)	F_4	B_1	F_1	82.8(17)
C_{14}	N_1	C_2	108.1(17)	N_4	C_6	C_7	102.4(18)
C_{14}	N_1	C_{15}	130.0(18)	C_{14}	C_{13}	N_2	106(2)
N_3	C_7	C_6	106.7(17)	C_{13}	C_{14}	N_1	113(2)
C_9	N_6	C_8	126.3(18)	C_{16}	C_{17}	C_{18}	80.1(18)

Table S6. Crystal data and structure refinement ^{Me}**Ph-Ir**$^{+}$.

Identification code	str2297_autored
Empirical formula	$C_{22}H_{26}F_6IrN_4O_4P$
Formula weight	747.64
Temperature/K	149.9(3)
Crystal system	monoclinic
Space group	$P2_1/c$
a/Å	9.6538(3)
b/Å	27.3149(8)

c/Å	10.2280(3)
α/°	90
β/°	90.034(3)
γ/°	90
Volume/Å^3	2697.05(14)
Z	4
ρ_{calc}g/cm^3	1.841
μ/mm^{-1}	10.852
F(000)	1456.0
Crystal size/mm^3	0.2 × 0.137 × 0.044
Radiation	Cu Kα (λ = 1.54184)
2Θ range for data collection/°	8.646 to 117.83
Index ranges	-9 ≤ h ≤ 10, -28 ≤ k ≤ 30, -11 ≤ l ≤ 11
Reflections collected	12867
Independent reflections	3732 [R_{int} = 0.0409, R_{sigma} = 0.0322]
Data/restraints/parameters	3732/0/350
Goodness-of-fit on F^2	1.061
Final R indexes [I>=2σ (I)]	R_1 = 0.0340, wR_2 = 0.0899
Final R indexes [all data]	R_1 = 0.0354, wR_2 = 0.0923
Largest diff. peak/hole / e Å^{-3}	1.86/-1.58

Table S7. Bond lengths for ^{Me}**Ph-Ir**$^+$.

Atom	Atom	Length/Å	Atom	Atom	Length/Å
Ir1	C2	2.063(8)	C15	C14	1.338(13)
Ir1	C1	2.087(7)	C14	N2	1.363(10)
Ir1	C4	1.898(10)	C1	N3	1.334(10)
Ir1	C3	1.877(12)	C1	N4	1.343(9)
P1	F4	1.591(5)	N3	C7	1.383(10)
P1	F2	1.604(4)	N3	C8	1.425(10)
P1	F5	1.577(5)	N2	C13	1.443(10)
P1	F1	1.577(5)	N4	C5	1.459(10)
P1	F3	1.591(6)	N4	C6	1.377(10)
P1	F6	1.605(5)	C7	C6	1.349(12)
C12	C11	1.395(13)	O1	C3	1.142(13)
C12	C13	1.380(13)	C4	O2	1.132(11)
C11	C10	1.362(14)	C13	C8	1.388(12)
C2	N1	1.347(10)	O4	C18	1.179(9)
C2	N2	1.361(11)	C19	C18	1.509(10)
N1	C15	1.381(10)	C18	C17	1.482(11)
N1	C16	1.460(11)	C21	C22	1.479(12)

Table S7. Bond lengths for ^{Me}**Ph-Ir**$^{+}$.

Atom	Atom	Length/Å	Atom	Atom	Length/Å
C9	C10	1.393(14)	C21	O3	1.168(14)
C9	C8	1.392(13)	C21	C20	1.453(15)

Table S8. Bond angles for ^{Me}**Ph-Ir**$^{+}$.

Atom	Atom	Atom	Angle/°	Atom	Atom	Atom	Angle/°
C2	Ir1	C1	82.9(2)	C14	C15	N1	106.5(7)
C4	Ir1	C2	177.0(4)	C15	C14	N2	106.9(7)
C4	Ir1	C1	94.1(4)	N3	C1	Ir1	124.5(5)
C3	Ir1	C2	92.7(4)	N3	C1	N4	106.5(6)
C3	Ir1	C1	175.5(4)	N4	C1	Ir1	128.9(5)
C3	Ir1	C4	90.2(4)	C1	N3	C7	109.8(6)
F4	P1	F2	89.8(3)	C1	N3	C8	126.6(7)
F4	P1	F6	88.9(4)	C7	N3	C8	123.5(7)
F2	P1	F6	89.3(3)	C2	N2	C14	111.7(7)
F5	P1	F4	89.0(3)	C2	N2	C13	123.7(7)
F5	P1	F2	178.7(3)	C14	N2	C13	124.5(7)
F5	P1	F3	89.9(3)	C1	N4	C5	125.8(7)
F5	P1	F6	91.2(3)	C1	N4	C6	110.0(6)
F1	P1	F4	179.1(4)	C6	N4	C5	124.1(6)
F1	P1	F2	89.5(3)	C6	C7	N3	106.9(7)
F1	P1	F5	91.7(3)	O2	C4	Ir1	179.4(9)
F1	P1	F3	90.3(4)	O1	C3	Ir1	177.2(10)
F1	P1	F6	90.5(3)	C7	C6	N4	106.6(7)
F3	P1	F4	90.3(4)	C12	C13	N2	117.2(9)
F3	P1	F2	89.5(3)	C12	C13	C8	121.2(8)
F3	P1	F6	178.6(4)	C8	C13	N2	121.4(9)
C13	C12	C11	119.9(9)	C9	C8	N3	118.9(9)
C10	C11	C12	119.1(9)	C13	C8	C9	118.5(8)
N1	C2	Ir1	130.1(6)	C13	C8	N3	122.5(9)
N1	C2	N2	103.4(7)	O4	C18	C19	121.0(7)
N2	C2	Ir1	126.4(5)	O4	C18	C17	123.3(7)
C2	N1	C15	111.5(6)	C17	C18	C19	115.6(6)
C2	N1	C16	124.7(7)	O3	C21	C22	121.4(10)
C15	N1	C16	123.6(7)	O3	C21	C20	118.5(10)
C8	C9	C10	119.7(9)	C20	C21	C22	119.9(10)
C11	C10	C9	121.5(9)				

Table S9. Crystal data and structure refinement for **[$^{Me}C_2H_4$-Ir][Br]**.

Identification code	24PFA001
Empirical formula	$C_{19.75}H_{32.6}BrIrN_4O_2$
Formula weight	630.21
Temperature/K	100.00
Crystal system	monoclinic
Space group	P2/n
a/Å	15.8821(15)
b/Å	10.1194(9)
c/Å	24.188(2)
α/°	90
β/°	101.932(4)
γ/°	90
Volume/Å^3	3803.5(6)
Z	8
ρ_{calc}g/cm^3	2.201
μ/mm^{-1}	9.148
F(000)	2457.0
Crystal size/mm^3	0.12 × 0.04 × 0.03
Radiation	MoKα (λ = 0.71073)
2Θ range for data collection/°	4.378 to 72.636
Index ranges	-26 ≤ h ≤ 26, -16 ≤ k ≤ 16, -40 ≤ l ≤ 40
Reflections collected	355155
Independent reflections	18462 [R_{int} = 0.0834, R_{sigma} = 0.0292]
Data/restraints/parameters	18462/0/365
Goodness-of-fit on F^2	1.044
Final R indexes [I>=2σ (I)]	R_1 = 0.0565, wR_2 = 0.1671
Final R indexes [all data]	R_1 = 0.0711, wR_2 = 0.1772
Largest diff. peak/hole / e Å^{-3}	8.02/-3.97

Table S10. Bond lengths for **[$^{Me}C_2H_4$-Ir][Br]**.

Atom	Atom	Length/Å	Atom	Atom	Length/Å
Ir1	C1	2.068(5)	N6	C22	1.464(9)
Ir1	C2	2.070(6)	N7	C21	1.476(9)
Ir1	C3	1.886(7)	N7	C14	1.351(8)
Ir1	C4	1.887(6)	N7	C20	1.384(9)
Ir1	Br1	2.9841(6)	N1	C2	1.373(8)
Ir2	C15	2.100(5)	N1	C13	1.472(9)
Ir2	C17	1.884(7)	N1	C12	1.378(9)
Ir2	C14	2.055(6)	N2	C2	1.358(8)

Table S10. Bond lengths for **[$^{Me}C_2H_4$-Ir][Br]**.

Atom	Atom	Length/Å	Atom	Atom	Length/Å
Ir2	C16	1.908(6)	N2	C10	1.482(9)
Ir2	Br2	2.9982(6)	N2	C11	1.376(9)
N4	C1	1.344(8)	N8	C19	1.377(9)
N4	C6	1.392(8)	N8	C14	1.348(8)
N4	C5	1.454(8)	N8	C18	1.473(9)
O4	C17	1.134(8)	C23	C24	1.338(10)
N5	C15	1.350(8)	C6	C7	1.351(11)
N5	C25	1.464(8)	C19	C20	1.330(12)
N5	C24	1.386(8)	C22	C21	1.477(9)
N3	C1	1.362(7)	C9	C10	1.500(10)
N3	C7	1.380(9)	C11	C12	1.326(11)
N3	C9	1.472(9)	C3	O1	1.147(8)
N6	C15	1.358(8)	O2	C4	1.143(8)
N6	C23	1.383(8)	O3	C16	1.139(8)

Table S11. Bond angles for **[$^{Me}C_2H_4$-Ir][Br]**.

Atom	Atom	Atom	Angle/°	Atom	Atom	Atom	Angle/°
C1	Ir1	C2	85.1(2)	N5	C15	N6	104.7(5)
C1	Ir1	Br1	105.31(16)	N6	C15	Ir2	130.9(4)
C2	Ir1	Br1	105.63(16)	C14	N7	C21	121.6(6)
C3	Ir1	C1	179.1(3)	C14	N7	C20	110.2(6)
C3	Ir1	C2	94.2(3)	C20	N7	C21	128.2(6)
C3	Ir1	C4	91.5(3)	C2	N1	C13	125.4(5)
C3	Ir1	Br1	75.4(2)	C2	N1	C12	111.2(5)
C4	Ir1	C1	89.1(2)	C12	N1	C13	123.3(6)
C4	Ir1	C2	172.4(2)	C2	N2	C10	130.6(6)
C4	Ir1	Br1	80.69(19)	C2	N2	C11	111.4(6)
C15	Ir2	Br2	109.50(16)	C11	N2	C10	118.0(6)
C17	Ir2	C15	176.4(3)	C19	N8	C18	125.5(6)
C17	Ir2	C14	92.3(3)	C14	N8	C19	110.1(6)
C17	Ir2	C16	92.4(3)	C14	N8	C18	124.3(6)
C17	Ir2	Br2	73.7(2)	N1	C2	Ir1	124.6(4)
C14	Ir2	C15	85.4(2)	N2	C2	Ir1	132.1(4)
C14	Ir2	Br2	102.14(17)	N2	C2	N1	103.1(5)
C16	Ir2	C15	89.8(2)	C24	C23	N6	108.1(5)
C16	Ir2	C14	175.2(2)	C7	C6	N4	107.1(6)
C16	Ir2	Br2	80.08(19)	O4	C17	Ir2	178.6(7)
C1	N4	C6	110.1(5)	C23	C24	N5	105.7(6)

Table S11. Bond angles for **[$^{Me}C_2H_4$-Ir][Br]**.

Atom	Atom	Atom	Angle/°	Atom	Atom	Atom	Angle/°
C1	N4	C5	125.8(5)	C6	C7	N3	106.7(5)
C6	N4	C5	124.0(6)	C20	C19	N8	107.6(7)
C15	N5	C25	126.6(5)	N6	C22	C21	116.5(5)
C15	N5	C24	111.6(5)	N7	C21	C22	113.2(6)
C24	N5	C25	121.6(5)	N3	C9	C10	114.4(6)
C1	N3	C7	110.5(6)	N7	C14	Ir2	123.0(5)
C1	N3	C9	121.6(5)	N8	C14	Ir2	131.4(4)
C7	N3	C9	127.9(6)	N8	C14	N7	105.3(5)
C15	N6	C23	110.0(5)	C19	C20	N7	106.8(6)
C15	N6	C22	131.3(5)	N2	C10	C9	116.8(6)
C23	N6	C22	118.7(5)	C12	C11	N2	107.4(6)
N4	C1	Ir1	130.3(4)	C11	C12	N1	106.8(6)
N4	C1	N3	105.6(5)	O1	C3	Ir1	178.2(7)
N3	C1	Ir1	124.1(4)	O2	C4	Ir1	176.4(6)
N5	C15	Ir2	124.4(4)	O3	C16	Ir2	178.3(6)

7. References

[1] A. M. Borys, *Organometallics* **2023**, *42*, 182–196.

[2] M. Monticelli, C. Tubaro, M. Baron, M. Basato, P. Sgarbossa, C. Graiff, G. Accorsi, T. P. Pell, D. J. D. Wilson, P. J. Barnard, *Dalton Transactions* **2016**, *45*, 9540–9552.

[3] M. Lee, Z. Niu, C. Slebodnick, H. W. Gibson, *Journal of Physical Chemistry B* **2010**, *114*, 7312–7319.

[4] J. L. Herde, J. C. Lambert, C. V. Senoff, M. A. Cushing, in *Inorganic Syntheses*, **1974**, pp. 18–20.

[5] S. Gonell, M. Poyatos, J. A. Mata, E. Peris, *Organometallics* **2012**, *31*, 5606–5614.

[6] G. R. Fulmer, A. J. M. Miller, N. H. Sherden, H. E. Gottlieb, A. Nudelman, B. M. Stoltz, J. E. Bercaw, K. I. Goldberg, *Organometallics* **2010**, *29*, 2176–2179.

[7] G. M. Sheldrick, *Acta Crystallogr C Struct Chem* **2015**, *71*, 3–8.

[8] O. V. Dolomanov, L. J. Bourhis, R. J. Gildea, J. A. K. Howard, H. Puschmann, *J Appl Crystallogr* **2009**, *42*, 339–341.